www.czasopisma.pan.pl PAN POLSKA AKADEMIA NAUK www.journals.pan.pl

A R C H I V E S O F M E T A L L U R G Y A N D M A T E R I A L S

Volume 60 2015 Issue 4

DOI: 10.1515/amm-2015-0414

W. PIEKARSKA*,#

NUMERICAL AND EXPERIMENTAL STUDY OF PHASE TRANSFORMATIONS IN WELDING PROCESSES

BADANIA NUMERYCZNE I DOŚWIADCZALNE PRZEMIAN FAZOWYCH W PROCESACH SPAWANIA

The paper concerns the mathematical and numerical modeling of phase transformations in solid state occurring during welding. The analysis of the influence of heating rate, cooling rate and maximum temperatures of thermal cycles on the kinetics of phase transformations is presented. On the basis of literature data and experimental studies the evaluation of classic mathematical and numerical models of phase transformation is presented with respect to the advanced methods of welding by using a high speed and a high power heat source. The prediction of the structure composition in laser welded butt-joint made of S460 steel is performed, where phase transformations are calculated on the basis of modified numerical models. Temperature distributions are determined as well as the shape and size of fusion zone and heat affected zone (HAZ). Temperature field is obtained by the solution of transient heat transfer equation with convective term and external volumetric heat source taken into account. Latent heat of fusion, evaporation and heats generated during phase transformations in solid state are considered in the numerical algorithm due to the large temperature range present in analyzed process. Results of the numerical prediction of structure composition in HAZ are presented in this work. Obtained results of computer simulations are compared to experimental research performered on the laser welded joint.

Keywords: Phase transformation, laser welding, numerical modelling, experimental research

Praca dotyczy modelowania matematycznego i numerycznego przemian fazowych w stanie stałym w procesie spawania. Przedstawiono analizę wpływu szybkości nagrzewania, szybkości chłodzenia oraz maksymalnej temperatury cyklu cieplnego na kinetykę przemian fazowych. W oparciu o dane literaturowe i badania doświadczalne przedstawiono weryfikację klasycznych modeli matematycznych i numerycznych przemian fazowych w odniesieniu do zaawansowanych metod spawania szybkobieżnym źródłem ciepła dużej mocy. Na bazie zmodyfikowanych modeli numerycznych przemian fazowych przedstawiono przykład prognozowania numerycznego składu fazowego doczołowego połączenia spawanego wiązką promieniowania laserowego ze stali S460. Wyznaczono rozkład temperatury, określono kształt i wielkość strefy przetopienia oraz strefy wpływu ciepła (HAZ). Pole temperatury uzyskano z rozwiązania równania przewodzenia ciepła z członem konwekcyjnym z uwzględnieniem objętościowego źródła ciepła. Ze względu na szeroki zakres temperatur, występujących w procesie spawania laserowego w algorytmie uwzględniono ciepło topnienia, parowania oraz ciepła przemian fazowych w stanie stałym. Podano wyniki prognozowania numerycznego składu fazowego w HAZ złącza spawanego. Wyniki symulacji komputerowej porównano z wynikami badań doświadczalnych połączenia spawanego.

1. Introduction

The material in the joint weld and adjacent region is heated to various temperatures in the welding process. As a result of different heating and cooling conditions a variety of structures occur in the joint, having different mechanical properties. Changes in the structure of heat affected zone covering phase transformations in solid state are the cause of significant changes in the properties of this zone in comparison to base material [1,2]. In the heat affected zone material is exposed to a very different thermal conditions and the resulting HAZ structure in welded steel highly depend on thermal cycle parameters, such as: heating rate, maximal heating temperature and cooling rate. In the analysis of phase transformations during welding the attention is mainly focused on phase transformations during cooling process [3-10]. The analysis of the kinetics of phase transformation is carried out by well known mathematical models found in the literature and Continuous-Cooling Transformations (CCT) diagrams. The analysis of phase transformations in the heating process in most cases is carried out for constant Ac_1 and Ac_3 temperatures, whereas the effect of the maximum heating temperature is substantially omitted [11-16].

The impact of both the heating rate and the maximum temperature of the thermal cycle on the kinetics of phase transformations during the welding process should be taken into account in the case of advanced welding methods by using a focused high power heat sources, such as: a laser

* INSTITUTE OF MECHANICS AND MACHINE DESIGN FOUNDATIONS, CZESTOCHOWA UNIVERSITY OF TECHNOLOGY, DĄBROWSKIEGO 73, 42-200 CZĘSTOCHOWA

Corresponding author: piekarska@imipkm.pcz.pl

beam welding or a laser-arc hybrid welding, where there are high heating rates as well as very high and various maximum heating temperatures of steel. Considering above facts, issues in the modelling of the kinetics of phase transformation in solid state are presented in this paper in relation to welding using a high speed and high power heat source. Mathematical and numerical models of phase transformation are presented as well as modified numerical models for the prediction of phase composition in welded joint, developed on the basis of literature data and experimental research. Presented in this paper research concerns structure composition of laser butt-welded joint made of S460 steel.

2. Phase transformations in heating and cooling processes

The analysis of phase transformations in continuous heating and cooling is carried out on the basis of models for non-isothermal disintegration of base phase as well as various analytical models [17-22]. A volumetric fraction of forming austenite during heating is described by Johnson-Mehl-Avrami (JMA) model, expressed as follows [23]:

$$\tilde{\eta}_A(T,t) = \eta_{(.)}(1-\exp(-bt^n)) \tag{1}$$

where $\eta_{(.)}$ is a sum of volumetric fractions of base material phase composition ($\eta_{(.)}$=1), coefficients $b=b(T)$ and $n=n(T)$ are determined by start (η_s=0.01) and final (η_f=0.99) conditions for phase transformations:

$$b(T) = -\frac{\ln(\eta_f)}{(t_s)^{n(T)}}, \quad n(T) = \frac{\ln\left(\ln(\eta_f)/\ln(\eta_s)\right)}{\ln\left(t_s/t_f\right)} \tag{2}$$

where t is a time, $t_s=t_s(T_{sA})$ and $t_f=t_f(T_{fA})$ are start and finish times of a phase transformation, T_{sA} and T_{fA} are corresponding start and finish temperatures.

Phase fractions forming during the cooling process are determined by the temperature and cooling rate $\left(v_{8/5} = \left(800^oC - 500^oC\right)/t_{8/5}\right)$ in the temperature range [800÷500]°C, where $t_{8/5}$ is a cooling time. A fraction of the new phase like: ferrite, pearlite and bainite (diffusive transformations) are determined on the basis of JMA formula taking into account already existing phase fractions:

$$\eta_{(.)}(T,t) = \eta_{(.)}^{\%}\tilde{\eta}_A\left(1-\exp\left(-b(t(T))^n\right)\right), \quad \tilde{\eta}_A = 1-\sum_k \eta_k \tag{3}$$

where $\eta_{(.)}^{\%}$ is the maximum fraction for determined cooling rate, estimated on the basis of microstructure analysis of examined steel, η_A is austenite fraction due to heating process, η_k is a phase fraction formed earlier in the cooling process, coefficients b and n are also determined using formula (2), in which $b=b(T(v_{8/5}))$ and $n=n(T(v_{8/5}))$.

Volumetric fraction of martensite (ηM) below M_s temperature is estimated according to the following Koistinen-Marburger (KM) equation [24]:

$$\eta_M(T) = \eta_{(.)}^{\%}\left(1-\exp\left(-k(M_s-T)\right)\right), \quad T \in \left[M_s, M_f\right] \tag{4}$$

Coefficient k depends on martensite phase start and final temperatures (M_s and M_f) determined also basing on CCT diagram:

$$k = -\frac{\ln(\eta_S)}{M_s - M_f} = -\frac{\ln(0.01)}{M_s - M_f} \tag{5}$$

The heating rate significantly affects the temperature of austenite formation. As a result of high heating rates up to the maximum temperature in the process (reaching hundred of K/s in submerged arc welding and several thousands K/s in laser or laser-arc hybrid welding) austenitization temperatures Ac_1 and Ac_3 significantly increase, wherein Ac_3 temperature grows more significantly (Fig. 1-3). This is confirmed by results of dilatometric studies on S460 steel and data from the literature [25]. Samples of 10mm length were used in all performed dilatometric tests.

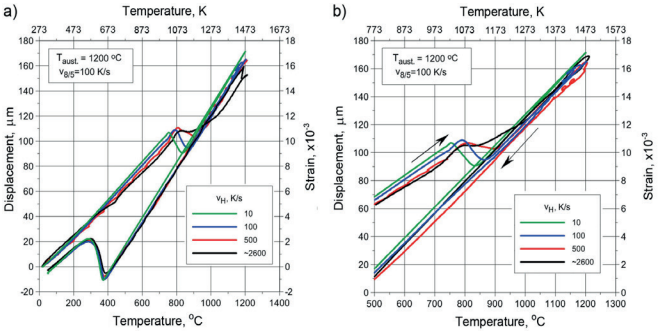

Fig. 1. Dilatometric curves for steel heated using different heating rates

The influence of heating rate on the increase of start and finish temperatures of the transformation α→γ may be different for different steels. It was found that temperatures Ac_1(t) and Ac_3(t) for a group of weldable high strength steels are rising at high temperatures on average 95÷110°C (Ac_1(t)) and 130÷180°C (Ac_3(t)). Temperature increase (ΔAc_3) as a function of heating rate for different weldable steels is illustrated in Fig. 2 [25]. Fig. 3 shows the change in temperatures Ac_1 and Ac_3 in S460 steel depending on the heating rate.

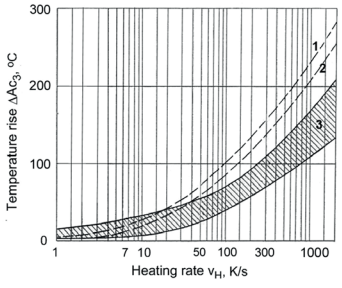

Fig. 2. The influence of heating rate on the increase of Ac_3 temperature: 1-structural steel (~0.4 %C), 2-alloy steel, 3-weldable, higher strength steel [25]

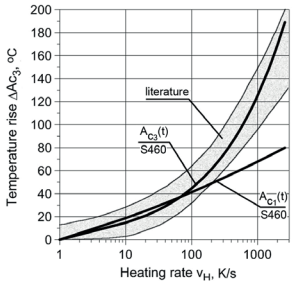

Fig. 3. The increase of Ac_1 and Ac_3 temperatures in S460 steel in the function of heating rates

The analysis of the kinetics of the austenite during heating is usually performed on the basis of dilatometric research. The influence of heating rates on Ac_1 and Ac_3 temperatures are

presented in Continuous-Heating-Transformation diagrams (CHT) for continuous heating at various rates (Fig. 4). However, this requires costly and time consuming experimental research. Authors of [26] developed CHT diagram for higher-strength steel heated at different rates. Further, by the use of equations of the kinetics of phase transformations and results of the experiment they gave a formula for temperature changes during heating in the function of heating rates:

$$Ac_{1,3}(t) = Ac_{1,3} + v_H \cdot t \qquad (6)$$

where $Ac_{1,3}$ are equilibrium temperatures (Ac_1 and Ac_3), v_H is a heating rate, t is a time above static Ac_1 and Ac_3 temperatures.

Given by authors of [26] formula (6) for the determination of temperatures Ac_1 and Ac_3 depending on the heating rates determines these temperatures with a good approximation. This is confirmed by the comparison of results of the experiment on S460 steel and temperatures obtained by formula (6) for lower heating rates (100 < K/s) as well as for a high heating rates (100 > K/s) (Fig. 4).

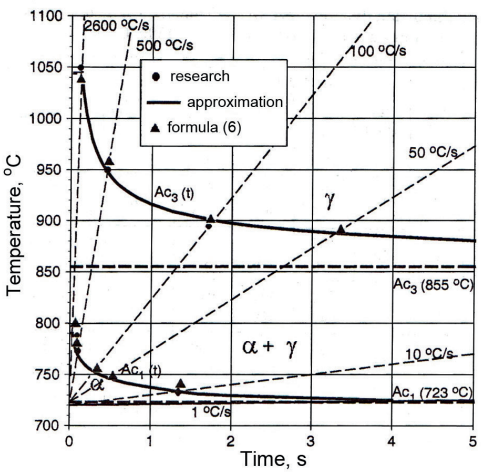

Fig. 4. Numerical and experimental CHT diagram of S460 steel

The type of phase transformations in the cooling process and the consequent changes in the specific volume, and in result the properties of HAZ, depend on cooling rates (Fig. 5a). The analysis of phase transformations during cooling in numerical solutions is carried out on the basis of mathematical models and CCT diagrams. The assessment of phase composition is obtained on the basis on the analysis of the microstructure, hardness testing of a set of samples and the analysis of dilatometric curves (Fig. 5b). CCT diagrams are used together with final fractions of phases corresponding to given cooling rates (Fig. 6), wherein cooling times ($t_{8/5}$) and cooling rates ($v_{8/5}$) are values determined in the temperature range of [800÷500]°C.

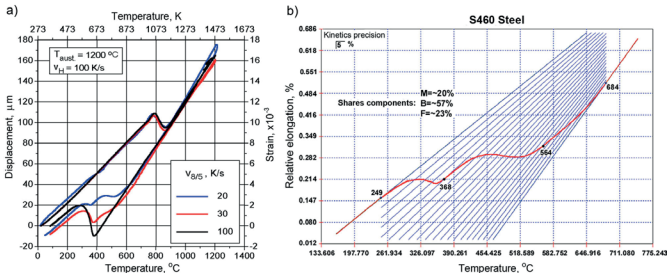

Fig. 5. Dilatometric curves a) for various cooling rates and b) quantitative interpretation of the phase composition of steel during continuous cooling by the analysis of dilatometric curve ($v_{8/5}$=20 K/s)

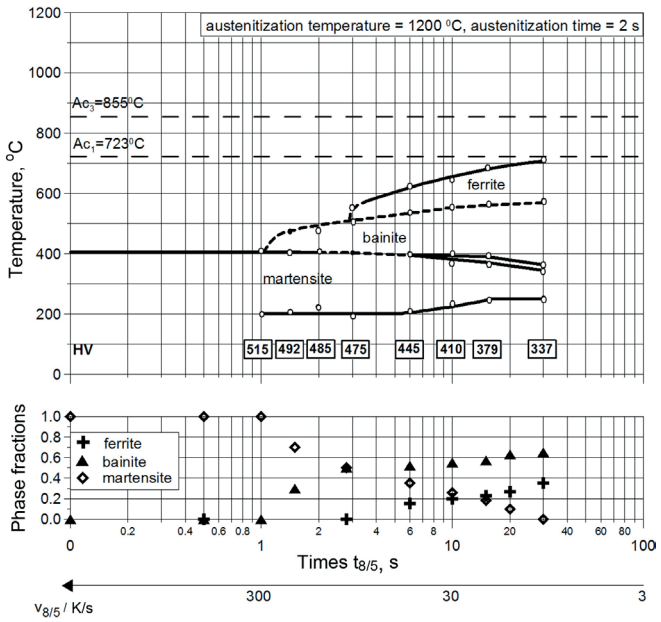

Fig. 6. CCT diagram of S460 steel and final fractions of microstructure constituents

A good approximation of start and final temperatures of phase transformations and the content of each phase can be achieved with the use of CCT diagram and phase composition corresponding to determined cooling rates. However, the determination of the kinetics of phase transformation according to applied mathematical models requires information about thermal dilatations of phases and the size of the volume changes during the transformations from one phase to another depending on cooling rates for particular steel. Reliable determination of structural transformations is obtained on the basis of experimental verification (Figs. 7-10). Simulated dilatometric curves for determined parameters of heating and cooling are compared with obtained experimentally dilatometric curves (Fig. 7 and Fig. 8).

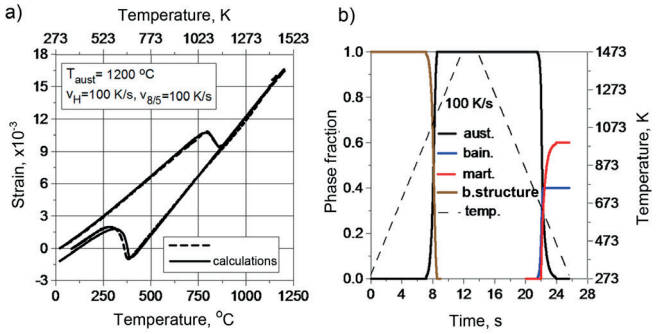

Fig. 7. Dilatometric curves a) and corresponding kinetics of phase transformations in S460 steel b) (v_H =100 K/s and $v_{8/5}$ = 100 K/s)

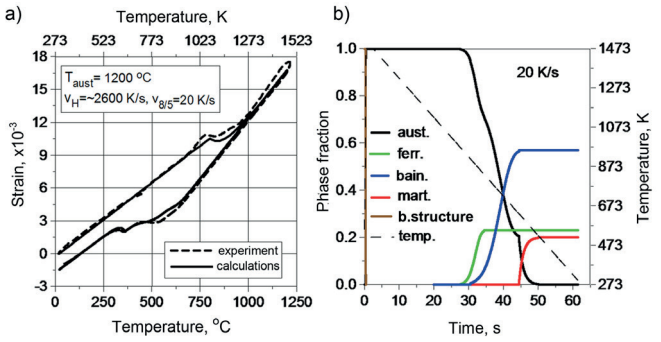

Fig. 8. Dilatometric curves a) and corresponding kinetics of phase transformations in S460 steel b) (v_H = 2600 K/s i $v_{8/5}$ = 20 K/s)

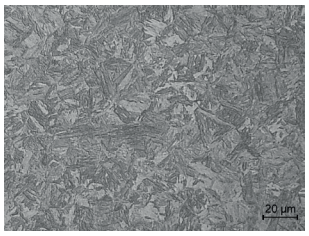

Fig. 9. Microstructure of S460 steel, bainite + martensite (v_H =100 K/s i $v_{8/5}$ = 100 K/s)

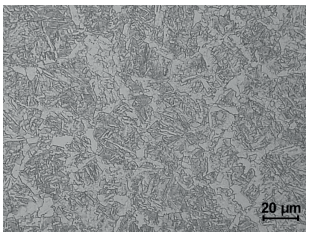

Fig. 10. Microstructure of S460 steel, ferrite + bainite + martensite (v_H = 2600 K/s i $v_{8/5}$ = 20 K/s)

Thermal expansion coefficients ($\alpha_{(i)}$=$\alpha_{(i)}$(T)) for different structural constituents and structural strains ($\varepsilon_{(i)}^{ph}$) induced by phase transformations are determined on the basis of experimental verification results. Values for S460 steel are given in Table 1.

3. The influence of austenitization temperature on phase transformations

The maximum temperature of steel heating has important impact on the kinetics of phase transformations occurring during cooling. Performed research has shown that higher heating temperatures result in lower temperatures of phases' initialization (Fig. 11).

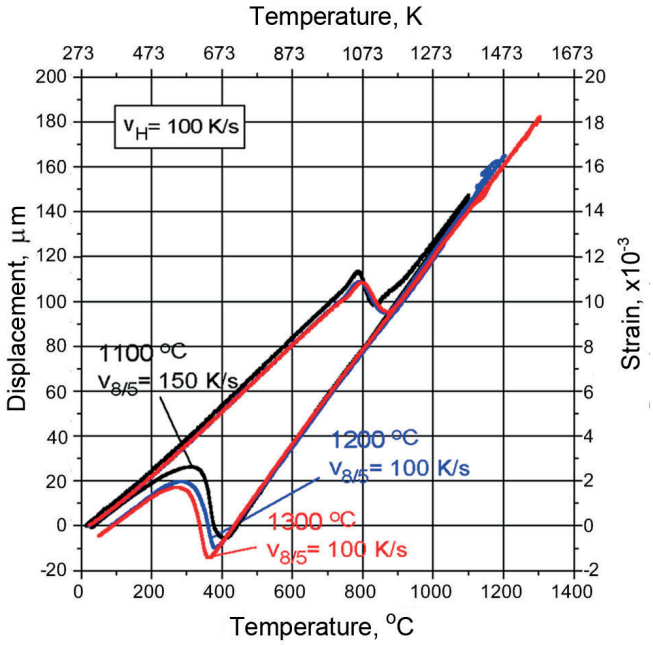

Fig. 11. Dilatometric curves of S460 steel at various austenitization temperatures

Such dependency is also shown in results of dilatometric tests conducted by authors of [27] for higher-strength steels and different heating temperatures, at assumed constant conditions of heating and cooling. A comparison of CCT diagrams shows that start and finish times of phase transformations in cooling process ($t_{8/5}$) are moving in the direction of shorter cooling times with lowering temperature of austenitization, identified with the maximum temperature of thermal cycle.

As a result, for various heating temperatures with the same cooling times ($t_{8/5}$) different structures are obtained. CCT diagram determined for only one austenitization temperature limits the analysis of structural changes in HAZ, especially in the case when very different heating temperatures are present. Only a creation of series of CCT diagrams, differing in maximum temperatures of thermal cycles allows for more accurate analysis of phase transformations in the entire area of HAZ.

On the basis of research conducted on the effects of maximum temperatures of thermal cycles on the kinetics of phase transformations it is possible to build CCT diagrams, showing changes in star times of each phase transformation in a function of the maximum temperature of thermal cycle

TABLE 1

Thermal expansion coefficients and structural strains

Structure constituent	Austenite	Ferrite	Pearlite	Bainite	Martensite
Thermal expansion coefficient, $\times 10^{-6}$ [1/K]	α_A=22.0	α_F=14.7	α_P=14.0	α_B=13.5	α_M=12.0
Isotropic structural strains, $\times 10^{-3}$	ε_A^{ph} =2.7	ε_F^{ph} =3.0	ε_P^{ph} =3.0	ε_B^{ph} =3.5	ε_M^{ph} =5.2

during welding which is called Maximum-Temperature-Cooling-Time diagram (Fig. 12). [27,28].

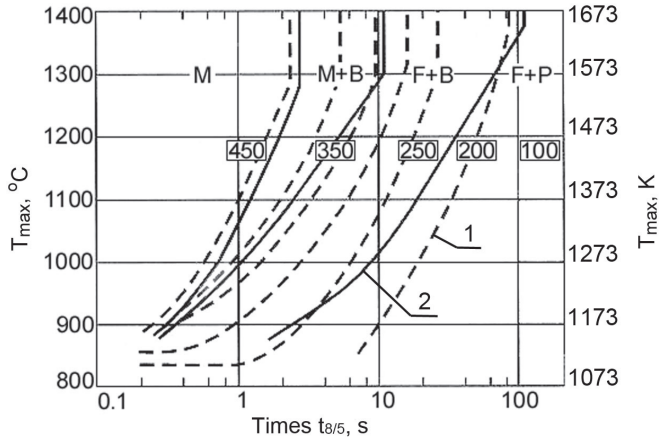

Fig. 12. Changes in start times of phase transformations in a function of maximum temperatures of thermal cycle in welding of low carbon steel, 1 - according to [27], 2 - according to [28]

As the maximum temperature increase in the thermal cycle during welding, start and finish times alternately move towards greater cooling times. Increasing the temperature above the austenitization temperature of 1300 °C wont affect significantly start and finish times of phase transformations. The amount of offset of start and finish times of phase transformations in the function of maximum temperatures of thermal cycles can be predicted using shifted CCT diagrams obtained for different austenitization temperatures. Unfortunately, these diagrams are very rare, mainly because of the cost of the research. Such studies are very time consuming and expensive, so they can not be universally useful. Most of CCT diagrams in welding that are used for the development of welding technology, is built for one heating temperature. This leads to certain approximations in predicting the structure composition in welded joints.

This work presents modelling of discrete CCT diagrams created on the basis of dilatometric research on S460 steel with the effect of austenitization temperature on the position of CCT diagram and thus the structural composition of analyzed steel taken into account. The mutual offset of two CCT diagrams for different austenitization temperatures is determined using experimentally obtained two CCT diagrams (Fig. 13) created by dilatometric research performed for two different austenitization temperatures (1100°C and 1200°C). A linear approximation of CCT diagrams offset is assumed along the time axis for different maximum temperatures of thermal cycles T_{max}=T_{aust} in the range of 1000°C÷1300°C using determined offset of CCT diagrams for austenitization temperatures 1100°C and 1200°C. The offset is described as follows:

$$t_B(T_{\max}) = t_B(1100) + \Delta t_B(T_{\max} - 1100)/100$$
$$t_F(T_{\max}) = t_F(1100) + \Delta t_F(T_{\max} - 1100)/100 \quad (7)$$

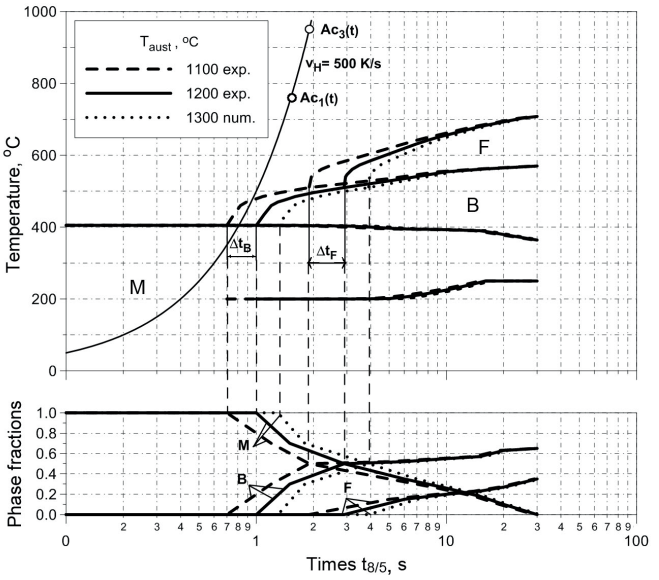

Fig. 13. The impact of austenitization temperatures on the location of CCT diagrams in S460 steel

The above analysis allowed the determination of a discrete form of the real CCT diagrams for arbitrary maximum temperatures of thermal cycles (model (7)). Different start and finish times of phase transformations are obtained for determined cooling rate ($v_{8/5}$) in welding, as a result of diagram offset with the maximum heating temperatures. However, presented approach requires a large number of dilatometric tests and this form can not be used as universal one.

In the numerical modelling of welding processes the approach requires an assurance that the model reflects real process conditions as much as it is possible, on the other hand developed models should be inexpensive and flexible. Therefore, simplified linear numerical model can be used for the consideration of the impact of austenitization temperature on the offset of CCT diagram (model (8)), considering a constant cooling rate (Fig. 14). This model assumes that relative linear offset of two graphs is proportional to the difference of austenitization temperatures corresponding to these diagrams. CCT diagram can be determined for any temperature $T_{aust} = T_{\max}^{T_i}$ by the use of experimentally prepared or taken from the literature CCT diagram determined for one chosen austenitization temperature (e.g. $T_{aust} = T_{\max}^{T_j} = 1200\ ^oC$ compare to Fig. 14), i.e. start and finish temperatures of ferrite and bainite transformations in a function of time ($(T_p(t_j)_{F,B}$), after assuming that $(T_p(t_j)_{F,B} = (T_p(t_i)_{F,B}$, are expressed as:

$$t_i(T_{\max})_{F,B} = \frac{(T_{\max} - T_p(t_i))t_i(T_{\max} = T_j)}{(T_{\max}^{T_j} - T_p(t_j))} \quad (8)$$

where T_p is a start temperature of a phase transformation.

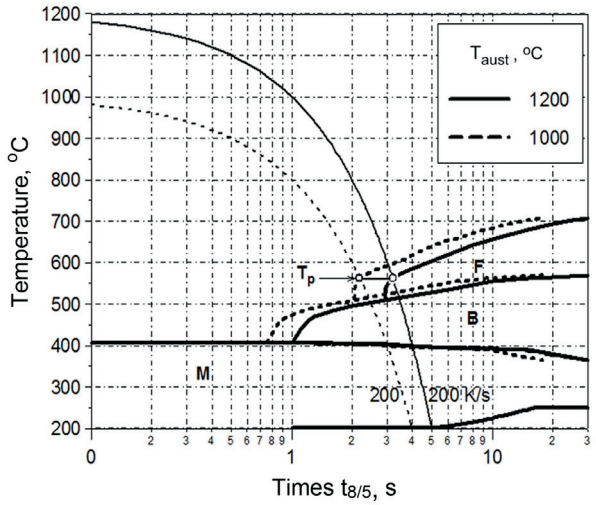

Fig. 14. Simplified model (model (8)) for the offset of CCT diagrams at different austenitization temperatures

Model (8) (Fig. 14) strikes an appropriate trends in offset of CCT diagrams with maximum temperatures of thermal cycles and it is possible to apply it for different steels having similar CCT diagrams. However, the use of linear simplified model (8) of diagram offset along time axis over the entire range of cooling rates for other steels with a greater diversity of structures requires further experimental verification.

4. Examples of numerical prediction of structure composition in welded joint

The temperature field in analyzed welding process is obtained on the basis of the numerical solution into transient heat transfer equation with convective term, taking into account heating of the workpiece by a laser beam volumetric heat source, phase transformations due to material state changes and phase transformations in solid state. Numerical analysis of laser but-welding without additional material is performed as a three-dimensional problem (Fig. 15a), assuming perfect contact between joined sheets. Analyzed domain with dimensions: L=250 mm, b=50 mm and g=5 mm is considered as a half of the joint to the plane of symmetry and discretized by differential grid with a constant spatial step of 0.01 mm in x direction and linearly decreasing spatial step in y direction (Fig. 15b) from 0.05 mm in the heat source activity zone, where large temperature gradients are present, up to 2 mm in lower temperatures. Following technological parameters are assumed in the analysis: laser beam power Q_L=3800 W, welding speed v=0.7 m/min, beam radius r_o=1 mm.

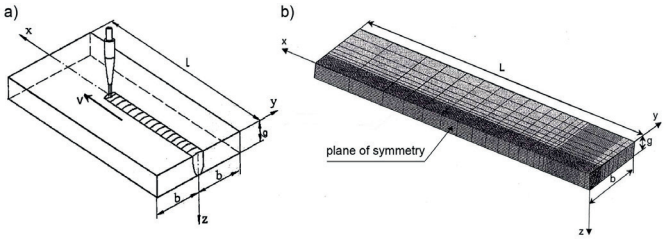

Fig. 15. Sketch of considered system: a) laser butt-welding process, b) difference element mesh used in calculations

Transient heat transfer equation in analyzed process is described in the following form:

$$\nabla\cdot(\lambda\nabla T)=C_{\mathrm{ef}}\left(\frac{\partial T}{\partial t}+\nabla T\cdot\mathbf{v}\right)-\widetilde{Q} \tag{9}$$

where $\lambda=\lambda(T)$ is thermal conductivity dependent on temperature, C_{ef} is effective heat capacity, $\widetilde{Q}$ is a volumetric heat source and $\mathbf{v}=\mathbf{v}(x,y,z,t)$ is a vector determined by welding speed, $T(x,y,z,t)$ is a temperature and t is time.

Equation (9) is completed by the initial condition $t=0: T=T_0$ and boundary conditions of Dirichlet, Neumann and Newton type, taking into account a heat loss due to convection and radiation [12]:

$$-\lambda\frac{\partial T}{\partial n}=-q+\alpha(T|_{\Gamma}-T_0)+\varepsilon\sigma(T^4-T_0^4) \tag{10}$$

where α is a convective coefficient (assumed as average value α=50 W/m^{2}K), ε=0.5 is a radiation coefficient, σ is Stefan-Boltzmann constant and $q=q(r,0)$ is the heat flux towards the top surface of welded workpiece ($z=0$) in the source activity zone, T_0=293 K is an ambient temperature.

Effective heat capacity is defined assuming linear approximation of solid fraction in the mushy zone and liquid fraction in liquid-gas region as well as the increase of a volumetric fraction of i-th phase in the solid state:

$$C_{ef}(T)=\begin{cases}\rho_S c_S+\sum_i \rho_S H_i^{\eta_i}\dfrac{d\eta_i(T)}{dT} & \text{for} \quad T\in\left[T_{st}^i;T_{fi}^i\right]\\ \rho_S c_S & \text{for} \quad T\notin\left(T_{st}^i;T_{fi}^i\right)\cup T<T_S\\ \rho_{SL}c_{SL}+\rho_S\dfrac{H_L}{T_L-T_S} & \text{for} \quad T\in[T_S;T_L]\\ \rho_L c_L & \text{for} \quad T\in[T_L;T_b]\\ \rho_L c_L+\dfrac{\rho_L H_b}{T_{\max}-T_b} & \text{for} \quad T\in[T_b;T_{\max}]\end{cases} \tag{11}$$

where subscripts S and L denote solid and liquid state, c is a specific heat (c_S=650 J/kgK, c_L=840 J/kgK), ρ is density (ρ_S=7800 kg/m^3, ρ_L=6800 kg/m^3), T_{st}^i and T_{fi}^i are start and finish temperatures of each phase transformation in solid state, $H_i^{\eta_i}$ is a latent heat of i-th phase transformation, η_i is a volumetric fraction of i-th phase, T_S=1750 K and T_L=1800 K are solidus and liquidus temperatures respectively, H_L=270x10^3 J/kg is a latent heat of fusion, T_b=3010 K is the boiling point of steel, T_{max} is the maximum temperature of thermal cycle, H_b=76x10^5 J/kg is a latent heat of evaporation. The product of density and specific heat in the mushy zone depends linearly on solid fraction $\rho_{SL}c_{SL}=\rho_S c_S f_S+\rho_L c_L(1-f_S)$, where $f_S\in[0;1]$ is the solid fraction.

Latent heats $H_i^{\eta_i}$ [J/kg] of the transformation of austenite into ferrite, pearlite and bainite in welded low carbon steel (according to authors of [29]) are approximated by the following square functions:

$$\begin{aligned} H_{A\to F}(T) &= -0.50315T^2 + 388.32T + 39652 \\ H_{A\to P}(T) &= -0.42990T^2 + 283.51T + 86588 \\ H_{A\to B}(T) &= -0.40676T^2 + 264.28T + 86860 \\ H_{A\to M}(T) &= H_{A\to B}(T) \end{aligned} \tag{12}$$

Gaussian heat source power distribution is developed for mushroom-shape welds (obtained during laser welding experiment). At the deep of penetration $\alpha_z d$ heat source power is decreasing in a shape of a truncated cone. Remaining laser power distribution is constant in a shape of a cylinder. Heat source power distribution in truncated cone volume is expressed as follows [30]:

$$Q(r,z) = \frac{\eta Q_L}{V}\exp\left[\left(1-\frac{r^2}{r_z^2}\right)\left(1-\frac{z}{d}\right)\right] \tag{13}$$

where Q_L is a laser beam power [W], η is efficiency, d is a total penetration depth, $r=\sqrt{x^2+y^2}$ is a current beam radius [m] and $z\in[0;\alpha_z d]$ is a current penetration [m], $V=\pi d\left(r_{\alpha z}^2\left(1-\frac{2}{3}\alpha_z\right)+\frac{1}{3}\alpha_z\left(r_0^2+r_0 r_{\alpha z}\right)\right)$ is a volume of the heat source [m^3]. r_z is a total laser beam radius along penetration direction [m], defined as: $r_z = r(z) = r_0 - (r_0 - r_{\alpha z})\frac{z}{\alpha_z d}$, where r_0 is a radius of laser beam spot at the top surface of the workpiece (z=0) and $r_{\alpha z}$ is a radius of the beam at the deep of penetration $z=\alpha_z d$, $\alpha_z\in[0;1]$ is experimentally defined coefficient depending on the welding speed.

Thermal conductivity coefficient changing with temperature is assumed in theoretical model (Fig. 16). In solid state $\lambda=\lambda(T)$ is defined according to data form the literature [12]. Much higher value of $\lambda(T)$ is assumed at high temperatures, which corresponds to the motion of liquid material in the welding pool. Effective heat capacity in solid state for chosen points at the top surface of the joint is shown in Fig. 17. It can be noticed that various effective heat capacity is obtained depending on the kinetics of phase transformations in solid state and different start and final temperatures determined for each cooling rate in the weld and HAZ.

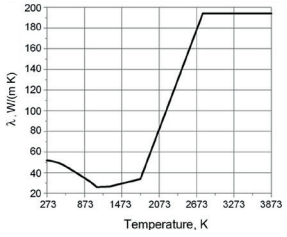

Fig. 16. Thermal conductivity assumed in calculations

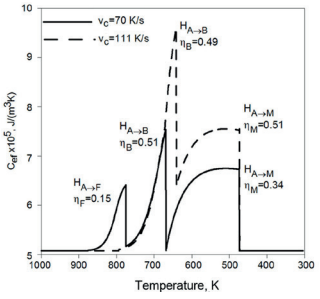

Fig. 17. Effective heat capacity for kinetics calculated for two chosen thermal cycles

Temperature field in the simulation of laser butt-welded steel sheets is obtained by the numerical solution of heat transfer equation (9) using finite difference method in forward Euler's time integration scheme. For the stabilization of solution algorithms Péclet number is implemented directly into central difference quotients. Numerical prediction of structure composition in the heat affected zone of welded joint is performed on the basis of the solution of equations (1), (3) and (4), using dynamic CCT diagrams (Fig. 13) according to model (7). In order to assess the suitability of model (8) comparative calculations using this model are also performed (Fig. 14).

If the maximum temperature T_{max} of thermal cycle is found between $[Ac_1 \div Ac_3]$ the case of incomplete austenitization is considered, assuming that the fraction of formed austenite equals:

$$\eta_A = (T_{\max} - Ac_1(t))/(Ac_3(t) - Ac_1(t)) \tag{14}$$

Remaining structure $(1-\eta_A)=\eta_k$ is a sum of volumetric fraction of base structure untransformed into austenite. In this case the summary fractions of phases arising during cooling are determined as a sum of fractions of given phases resulting from austenite and a fraction of this phase untransformed into austenite.

Figure 18 shows temperature distribution for chosen points at the top surface of the joint (z=0) and in a distance y=1 mm from the centre of laser beam heat source, where solidus, liquidus and boiling temperatures are marked as well as temperature range $[800^oC;500^oC]$ where cooling rates are determined for analysis of phase transformations in solid state.

In this figure maximum temperatures are observed in the centre of heat source activity zone. At this point temperature exceeds the boiling point of steel (T_b), leading to the evaporation and creation of the keyhole. When maximum temperature exceeds austenitization temperature (T_g), structural transformations appear (HAZ). Below austenitization temperature welded material is treated as untransformed base material.

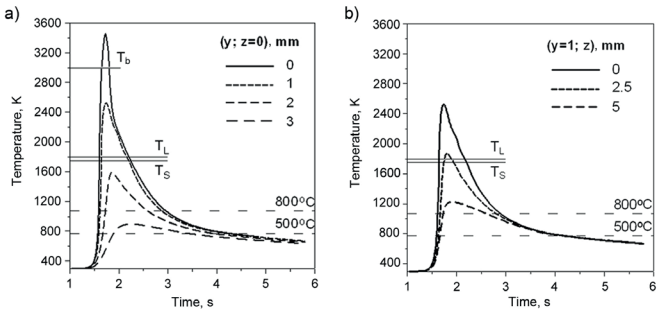

Fig. 18. Temperature distribution for chosen points: a) at the top surface of the weld and b) along direction material penetration, in a distance y=1 mm from the centre of laser beam heat source

In order to verify the correctness of elaborated models, CO_2 laser welding experiment is performed at Welding Institute in Gliwice. Laser butt-welding of sheets made of S460 steel is performed using TRUMPH Lasercell 1005 with CO_2 laser generator (Q_L=3800 W). Steel sheets dimensions are set to: 250x50x5 mm. Joined elements are arranged along the longest side without a gap (perfect contact). Welding speed is set to 0.7 m/min.

Figure 19a shows the comparison of experimentally obtained weld with numerically estimated melted zone and heat affected zone geometries. Microstructure at the junction of the weld and HAZ and in HAZ is presented in Fig. 19b and Fig. 19c. Figure 20 presents hardness distribution in the joint with corresponding measurement points.

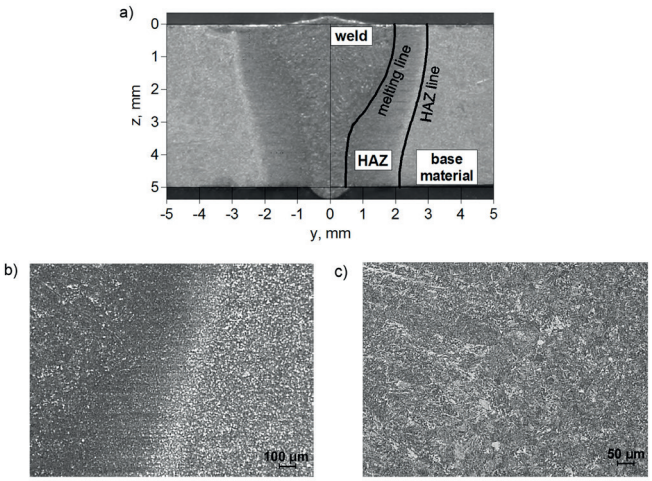

Fig. 19. Results of analysis: a) the comparison of numerically predicted melted zone and HAZ geometry with weld obtained by the experiment, b) microstructure of transition zone joint-HAZ and c) microstructure in HAZ

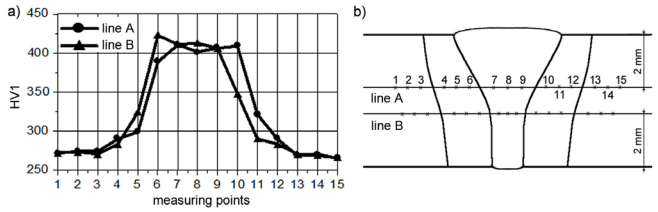

Fig. 20. Hardness in the cross section of the joint: a), scheme of the arrangement of hardness measurement points in the weld b) (v=0.7 m/min)

Figs. 21-22 present exemplary numerical results of the kinetics of phase transformation in welded joint. It is assumed on the basis of microscopic examinations that the base structure (parent material) is bainitic - ferritic structure, containing 60% of bainite and 40% of ferrite. The kinetics of phase transformation in HAZ at the distance y=1.5 mm from the heat source centre, respectively for the middle and lower surfaces of the joint is shown in Fig. 21. In the middle surface, for the same distance form the centre of the heat source (y=1.5 mm), a full transformation form base structure into austenite takes place (Fig. 21a), whereas in the lower surface (Fig. 21b) - only partial transformation (incomplete austenitization).

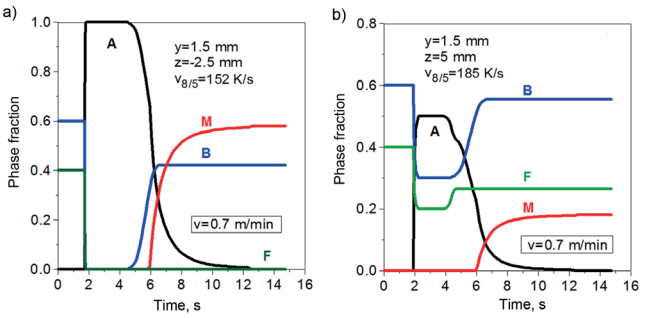

Fig. 21. Kinetics of phase transformations a) in the middle surface and b) lower surface of welded joint

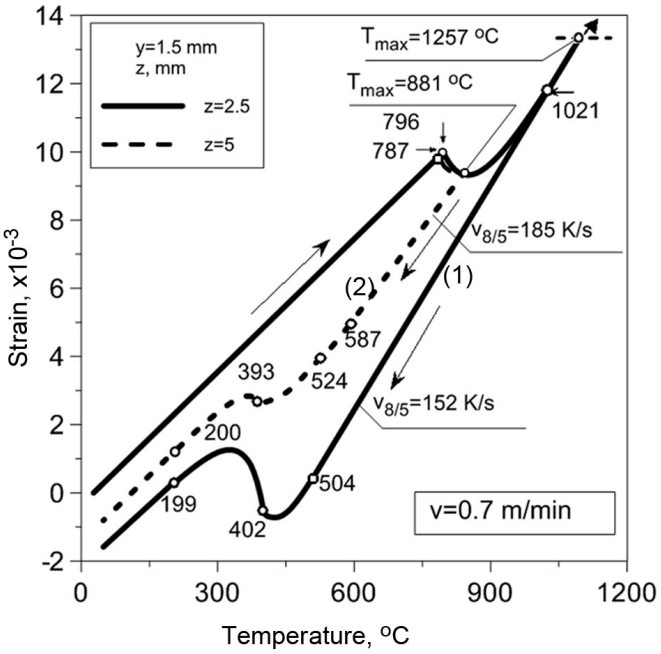

Fig. 22. Calculated dilatometric curves corresponding to the kinetics of phase transformations: 1 - Fig. 21a, 2 – Fig. 21b

Fig. 22 shows calculated dilatometric curves corresponding to the kinetics of phase transformations during heating and cooling (shown in Fig. 21). In this figure selected start and finish temperatures of phase transformations are marked, which were calculated on the basis of CHT and CCT diagrams for specified heating and cooling rates. The impact of austenitization temperature (model (7)) on the position of CCT diagram (diagram offset) is taken into account. Linearly offset of CCT diagrams correspond to different heating temperatures (1257°C and 881°C, see. Fig. 22). There are significant differences in the kinetics and the final structure for relatively small differences in the cooling rates, which is partly the result of diagram offset. The numerical prediction of the structure composition in the cross section of welded joint in the form of isolines of volume fractions of phases is shown in Fig. 23.

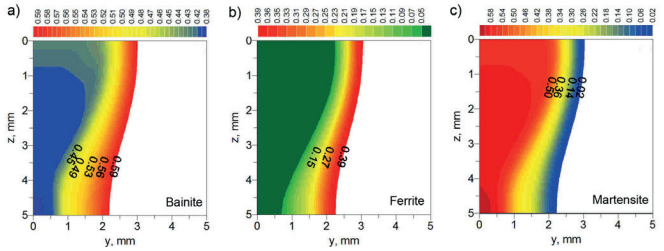

Fig.23. Volumettric fractions of bainite, ferrite and martensite phase in the cross section of welded joint

Used in this work model of CCT diagram offset along the time axis (model (7)) requires experimental confirmation. Simpler model (8) can be used with a good approximation and does not require additional research. Calculations made by these two models do not give significant differences in obtained results for analyzed cooling rate (Fig.24).

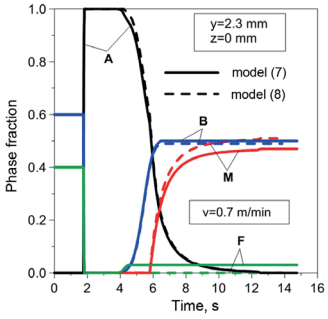

Fig. 24. Comparison of the kinetics of phase transformations in HAZ. Model (7) and model (8)

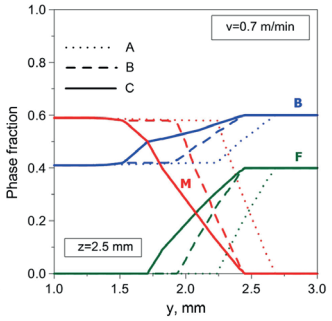

Fig. 25. Comparison of changes in the structure composition for used models

The structure of HAZ is determined in order to demonstrate the effect of austenitization temperature and heating rate on the kinetics of phase transformations during cooling. The prediction is performed according to three options: model A - using CCT diagram for one austenitic temperature T_a=1300°C and constant A_{c1} and A_{c3} temperatures; model B - using CCT diagram for one austenitization temperature of 1300°C and changing A_{c1}(t) and A_{c3}(t) temperatures; model C - using the model including the effect of austenitization temperature on the position of CCT diagram along the time axis (model (7), see. curves A-C in Fig. 25). The use of CCT diagram determined for one temperature (1300°C) gives a little various structures and inflated values of martensite. Consideration of different austenitization temperatures in the analysis of the kinetics of phase transformations leads to the reduction of the content of hardening structures in calculations and the offset of hardened zone.

5. Conclusions

Welding of steel using a single laser beam or laser-arc hybrid methods, in which large heating and cooling rates occur as well as greatly different maximum heating temperatures, require a modified approach to numerical modelling of phase transformations. The analysis of the kinetics of phase transformation during heating process should be carried out using CHT diagram, as shown by the experimental research and studies of the literature. The use of static CCT diagrams in some cases may lead to large differences in the predicted structure composition of the joint in comparison to the real weld. A closer specification of structure composition in the numerical modelling of cooling process is obtained on the basis of Maximum-Temperature-Cooling-Time diagram. Good quality results are achieved by the use of dynamic, discrete CCT diagrams. Models (7) and (8) proposed in this work cover the offset of the diagram along the time axis. Numerically estimated structure composition by using discrete "movable" diagrams for any maximum temperature of the thermal cycle with corresponding phase composition in welded joint, together with the interpretation of hardness distribution shows that consideration of the effect of different austenitization temperatures in the modelling of the kinetics of phase transformations in solid state has a great importance in the prediction of structural changes.

REFERENCES

[1] Y.C. Kim, M. Hirohata, K. Inose, Welding in the World, no **3**, 64 (2012).
[2] J. Pilarczyk, Metaloznawstwo spawalnicze, Wyd. Pol. Warszawskiej, Warszawa (1977).
[3] V.I. Makhnenko, G.Y. Saprykina, Paton Weld. J. **3**, 14 (2002).
[4] S. Serajzadeh, J Mater Process Tech. **146**, 311 (2004).
[5] K. Fanrong, M. Junjie, K. Radovan, J Mater Process Tech. **211**, 1102 (2011).
[6] Ch. Yongxiong, L. Xiubing, L. Yan, X. Binshi:, Materials & Design **31**, 3852 (2010).
[7] A. Bokota, W. Piekarska, Paton Weld. J, **6**, 19 (2008).
[8] V.I. Makhnenko, Pascetnyje metody issledovanija kinetiki svarocnych naprjazenij i deformacij, Kiev, Nauk. Dumka (1976).
[9] A.P. Mackwood, R.C. Cafer, Opt Laser Technol. **37**, 99 (2005).
[10] T.L. Chen, Y.H. Guan, H.G. Wang, J.T. Zhang, J Mater Process Tech. **63**, 546 (1997).
[11] J. Pilarczyk, M. Banasik, J. Stano, Przeglad Spawalnictwa **5-6**, 6 (2006).
[12] W. Piekarska, M. Kubiak, A. Bokota, Arch Metall Mater. **56**, 409 (2011).
[13] S.A. Tsirkas, P. Papanikos, Th. Kermanidis, J Mater Process Tech. **134**, 59 (2003).
[14] D. Gery, H. Long, P. Maropoulos, J Mater Process Tech. **167**, 393 (2005).
[15] J Słania., Arch Metall Mater. **3**, 757 (2005).
[16] P. Lacki, K. Adamus, K. Wojsyk, M. Zawadzki, Z. Nitkiewicz, Arch Metall Mater. **56**, 455 (2011).
[17] O. G. Kasatkin, P. Seyffart, Avtomat. Svarka **1**, 7 (1984).
[18] P. Seyffarth, O. G. Kassatkin, Schweißtechnik **29**, 117 (1979).
[19] O. Grong, Metallurgical Modelling of Welding, The Institute of Materials, Cambridge (1997).
[20] S. Serajzadeh, J Mater Process Tech. **146**, 311(2004).
[21] W. Zhang, B. Wood, T. DebRoy, et al., Acta Mater. **51**, 3333 (2003).
[22] Mathematical Modelling of Weld Phenomena, ed. H. Cerjak, K.E. Easterling, The Institute of Materials, Cambridge (1993).
[23] M.J. Avrami, Chem. Phys., 7, 1103-1112, (1939) Atlas of Time –Temperature Diagrams for Irons and Steels, ed. V. Voort G.

F., USA, ASM International, USA (1991).
[24] D.P. Koistinen, R.E. Marburger, Acta Metall. **7**, 59 (1959).
[25] M H. Sorsorov, Fazovye prevrascenia i izmenenia svojstv stali pri svarke, atlas, isd. Nauka, Moskva (1972)
[26] J.W. Elmer, T.A. Palmer, W. Zhang, B. Wood, T. DebRoy, Acta Mater. **51**, 12, 3333 (2003).
[27] C.F. Berkhout, P.H. van Lent, Schweißen und Schneiden, **6**, 256 (1968).
[28] K. Röhrs, V. Michailow, H. Wohlfahrt, Proc. of Int. Conference Mathematical Modelling and Information Technologies in Welding and Related Processes, Katsiveli, Crimea, Ukraine, ed. V.I. Makhnenko, E.O. Paton Welding Inst. of NAS of Ukraine, Kiev, 92 (2002).
[29] K.J. Lee, Scripta Mater. **40**, 735 (1999).
[30] W. Piekarska, M. Kubiak, Therm. Anal. Calorim. **110**, 159 (2012).

Received: 20 November 2015.